

# Universal route to optimal few- to single-cycle pulse generation in hollow-core fiber compressors

E. Conejero Jarque<sup>1,\*</sup>, J. San Roman<sup>1</sup>, F. Silva<sup>2,3</sup>, R. Romero<sup>2,3</sup>, W. Holgado<sup>1,+</sup>, M.A. Gonzalez-Galicia<sup>1</sup>, I.J. Sola<sup>1</sup>, H. Crespo<sup>2,1</sup>

**1** Grupo de Investigación en Aplicaciones del Láser y Fotónica, Departamento de Física Aplicada, University of Salamanca, E-37008, Salamanca, Spain.

**2** IFIMUP-IN and Departamento de Física e Astronomia, Faculdade de Ciências, Universidade do Porto, R. do Campo Alegre 687, 4169-007 Porto, Portugal.

**3** Sphere Ultrafast Photonics, S.A., R. do Campo Alegre 1021, Edificio FC6, 4169-007 Porto, Portugal.

**+** Present address: Centro de Laseres Pulsados, CLPU, Parque Científico, Villamayor, Spain.

**\*** enrikecj@usal.es

## Abstract

Gas-filled hollow-core fiber pulse post-compressors capable of generating few- to single-cycle pulses are a key enabling tool for attosecond science and ultrafast spectroscopy. Achieving optimum performance at such short pulse durations can be extremely challenging since it requires both the means to compensate the spectral phase of the pulses over ultra-broad bandwidths and an adequate temporal diagnostic. Although output spectra capable of supporting single-cycle pulse durations can be obtained at the output of a hollow-core fiber starting from the sub-30-fs pulses delivered by many commercial amplifiers available today, the above difficulties have hindered the full exploitation of the potential of such systems, namely the generation of stable and reproducible Fourier-transform limited pulses. In this work we show that, independently of conditions such as the type of gas or the laser system used, there is a universal route to obtain the shortest stable output pulse down to single-cycle durations. Numerical simulations and experimental measurements performed with the dispersion-scan technique reveal that, in quite general conditions, the best performance results in the post-compressed pulses typically exhibiting a residual third-order dispersion which is intrinsic to optimum nonlinear propagation within the fiber. The understanding of this effect and its adequate correction, e.g. using simple transparent optical media, enables achieving optimized high-quality post-compressed pulses with only minor changes in existing setups. These optimized sources have impact in many fields of science and technology and are an enabling technology for exciting new applications such as dual-color pump-probe spectroscopy in the sub-5-fs regime and novel laser-plasma particle accelerators.

## Introduction

The chirped pulse amplification (CPA) technique applied to Titanium Sapphire lasers has made intense near-infrared (NIR) ultrashort pulses in the 20 – 100 fs range widely available for scientific, biomedical and industrial applications. Special efforts have been devoted to generate even shorter pulses, in the few- and single-cycle regime, due to their potential applications and interest. In particular, such pulses have paved the way for attosecond physics and metrology [1–6], via the extreme ultraviolet (XUV) attosecond pulse trains and isolated attosecond pulses [7] that can be obtained by high-harmonic generation (HHG). The use of few-cycle optical pulses with durations close to or shorter than 10 fs in the near-infrared, visible and near-ultraviolet spectral regions has been extended in recent years to a wide range of spectroscopic techniques such as impulsive

---

vibrational spectroscopy [8–10], time-resolved stimulated Raman spectroscopy [11–14], and ultrafast pump-probe absorption spectroscopy [15, 16]. Few-cycle optical pulses have also become an interesting tool for transient absorption microscopy [17], near-field imaging techniques [18] and for generating ultrashort terahertz radiation [19].

While it is possible to obtain sub-10 fs pulses from CPA [20] or from optical parametric amplification [21] systems, the former is not easy to accomplish, and the latter is not commonplace. Therefore, post-compression techniques are usually employed for the generation of intense few- and even single-cycle pulses in the near- and mid-infrared spectral regions [22, 23]. In order to post-compress ultrafast pulses down to the few-cycle regime, two steps are usually needed. First, nonlinear processes broaden the pulse spectrum, thus decreasing the Fourier limited pulse duration. In a second step, the spectral phase resulting from the previous stage is compensated, typically using chirped mirrors, gratings, prisms, and other dispersive systems, resulting in a temporally compressed pulse. This scheme was first proposed in the context of optical fibers in the 1980s [24], and enabled achieving 6 fs pulses when compensating simultaneously the outcoming group delay dispersion (GDD) and third-order dispersion (TOD) [25]. The scheme was successfully expanded in 1996 by Nisoli and coworkers to the ultra-intense laser pulse regime (mJ-level pulses) by using hollow-core fibers (HCF) filled with gases [26]. Using the latter scheme, together with chirped mirrors as the compression system, few-cycle pulses in the hundreds of  $\mu\text{J}$  energy range with 0.1 TW peak power were obtained [27]. Later, similar results were obtained using the light filamentation process in the spectral broadening stage [28].

In spite of requiring a finer input beam alignment than filamentation-based compressors, HCF compressors are today the most widely used high-energy post-compressed sources, in part due to their intrinsic spatial filtering properties which result in very high quality beam profiles. Furthermore, their long-term stability can be greatly improved by using, e.g., piezo-driven mirror mounts to ensure stable and constant spatial coupling of the input laser pulses into the HCF via a simple feedback loop. Hollow-core fiber post-compressed pulses have shown a great potential in a wide range of applications, such as pump-probe experiments in conjunction with attosecond pulses [29], ultrafast measurement of electric and optical properties of solids [30, 31], time-resolved Coulomb explosion dynamics [32], ultrafast spectroscopy techniques [33–39], and very recently a new generation of compact kHz laser-plasma accelerators based on single-cycle pulses [40].

To access the Fourier Limit of a pulse after a nonlinear propagation process one has to deal with the complex phase that the pulse acquires due to the interplay of different linear and nonlinear effects. In general, researchers optimize their HCF compressors by empirically adjusting several key parameters, such as gas type and pressure, input pulse characteristics and coupling conditions, with the final result usually involving a delicate compromise between output efficiency, amount of spectral broadening and achievable degree of compression (pulse duration and quality) for their particular system and chirped mirror set. The ability to measure and quantify the achieved degree of compression is therefore paramount to identify the main characteristics of the output pulse and to further optimize its compression, e.g., by correcting residual phase errors whenever possible. Recently, additional optical elements have also been employed, in addition to the usual chirped mirrors, for added control over the compression. For instance, unusual materials like water [41], z-cut KDP [42] or z-cut ADP [6] crystals can be used for broadband TOD optimization, allowing the generation of single-cycle pulses by purposely not matching the GDD/TOD ratio of the chirped mirrors (which do not take the full nonlinear phase into account) and hence compensating the phase of the output pulse. Both spectral phase oscillations and the overall spectral phase of a pulse can be visualized in a very straightforward way using the dispersion-scan (d-scan) [43] technique, which has been extensively used in the last years to characterize many state-of-the-art few-cycle pulse sources around the world and is enabling new and very promising applications [6, 38–40, 46].

D-scan is a recent approach for the simultaneous measurement and compression of femtosecond laser pulses. Its experimental setup is fully in-line and does not require beam splitting and recombination nor temporal delay of short pulses. Experimentally it involves the measurement of the spectrum of a nonlinear signal such as second-harmonic generation (SHG) as a function of dispersion applied to the pulse. This can be performed with pulse compression setups, such as a chirped mirror (CM) and glass wedge compressor, where the amount of glass traversed by the pulse is an independent variable controlled by insertion of one of the wedges: while the CMs impart negative dispersion, the variable positive dispersion introduced by the wedges will vary the total dispersion experienced by the pulse to be measured. In second-harmonic generation d-scan (SHG d-scan), measuring the SHG signal after the compressor provides a two-dimensional trace of the SHG spectrum vs.

insertion. An optimization algorithm is then used to retrieve the spectral phase of the pulse from the measured d-scan trace and calibrated linear spectrum [43]. A recent approach to d-scan retrieval can also be used to obtain the pulse amplitude and phase from the measured trace [44], but in this case, the trace itself must be calibrated. D-scan has been successfully demonstrated with few-cycle pulses since its inception [22, 43], and over octave-spanning single-cycle pulses have been measured directly with SHG d-scan [6, 40–42, 44].

Apart from its robustness and performance, another important advantage of d-scan is the fact that it directly results in very intuitive traces that provide useful guiding information on the quality of the achieved pulse compression, which motivates our use of the d-scan trace as a diagnostic tool. For instance, a flat and thin trace is indicative of excellent compression, since this means that for a particular position of the compressor, all spectral components are equally compressed and hence their SHG signal is maximized. If the trace has a tilt, this means that different parts of the spectrum are being compressed for different dispersions. In other words, we have a frequency-dependent chirp in the pulses, i.e., the pulses have residual third-order dispersion. A curved, parabolic-like trace would be indicative of fourth-order dispersion, and so on. In the case of phase oscillations, these will also produce a wavy appearance in the resulting d-scan trace (for a more detailed description of d-scan traces and their interpretation, the reader is referred to refs. [22, 43]).

In this paper we look for a route to obtain the optimum stable post-compressed pulse from a HCF using the d-scan technique as the compression device and the d-scan trace to univocally identify this route. Numerical simulations and experimental measurements reveal that, in quite general conditions, the best performance results in the post-compressed pulses typically exhibiting a residual third-order dispersion of nonlinear origin, i.e., a signature TOD which is intrinsic to optimum nonlinear propagation within the fiber, in agreement with experimental observations made in several laboratories around the world. Overdriving the HCF above this optimum regime invariably results in an increasingly complex nonlinear spectral phase, partly due to plasma onset, which renders compression very hard to optimize. The understanding of this effect and its subsequent correction using, e.g., unusual transparent optical media with adequate ratio between second- and third-order dispersion, enables achieving optimized high-quality post-compressed pulses with only minor changes in existing setups.

## Results and Discussion

### Regimes of nonlinear propagation in the hollow-core fiber

The identification of the optimum parameters of a nonlinear process to obtain a desired output pulse is not an easy task. Fortunately, in the context of nonlinear propagation of ultrashort laser pulses, we have helpful theoretical models to guide us. We used a nonlinear spatio-temporal model (see the Methods section) to simulate the nonlinear propagation of laser pulses in a static HCF filled with different gases (argon, neon and air) and in different conditions (gas pressure; input pulse energy, chirp and duration) and their subsequent compression with a d-scan composed of chirped mirrors and glass wedges. All cases studied are representative of real experimental situations and present qualitatively similar dynamics. In Fig. 1 we present the evolution of different pulse and gas features during the nonlinear propagation of a laser pulse with a full-width at half-maximum (FWHM) duration of  $\sim 24$  fs, centered at 800 nm, in a hollow-core fiber of  $300\ \mu\text{m}$  core diameter. As relevant examples, we consider a 0.15 mJ laser pulse propagating in a HCF filled with Ar at 0.5 bar (blue continuous line), and a 0.6 mJ laser pulse propagating in a HCF filled with Ne at 1.5 bar (red dashed line). The parameters have been chosen so that optimum pulse compression for both gases occurs at the same HCF length.

In Fig. 1a) we see that both cases exhibit nonlinear spatial dynamics inside the HCF, presenting changes in the beam waist along propagation. This situation justifies using a spatio-temporal model for these conditions, regardless of the intrinsic guiding properties of the HCF. Regarding the spectro-temporal evolution, both gases present similar dynamics showing three different main propagation stages. The first stage, plotted over a cyan background in Fig. 1, is the start-up regime where the spectro-temporal evolution is monotonous and few changes appear. The second stage, plotted over green, is where all the accumulated nonlinear effects start to smoothly modify the spatio-temporal pulse structure. Here we observe the self-focusing of the beam (Fig. 1a) and an important spectral broadening (Fig. 1b), together with a temporal duration reduction (Fig. 1c), all the above without a significant contribution from the free electron density (everything occurring before the first

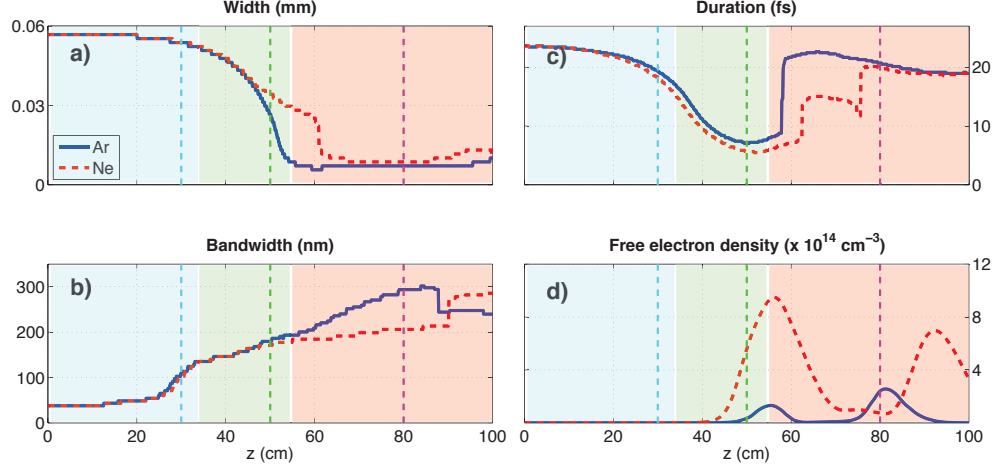


**Figure 1.** Nonlinear propagation dynamics for argon (blue continuous line) and neon (red dashed line). We show a) the spatial width of the beam, b) the pulse bandwidth, c) the temporal duration and d) the maximum free electron density, during propagation inside the HCF. Note: all widths are calculated as full width at half maximum (FWHM) quantities (see Methods section for more details), which show discontinuities as the pulse and spectrum become more structured (e.g., strong pre- and/or post-pulses develop in the temporal domain that can surpass the half-maximum of the main peak), although the corresponding evolution is perfectly continuous, as also evidenced in the video provided as Supplementary Material.

plasma peak, Fig. 1d). In the last stage, plotted over magenta, the dynamics becomes complex and rapidly-changing due to the effects induced by the plasma peaks generated in the HCF. In this stage the pulses acquire complicated spatio-temporal structures that change with the propagation distance.

In spite of the increasing spectral bandwidth, the evolution of the laser pulse structure in this last stage is hard to manage and is practically useless, if one is looking for a controllable, repeatable and high-quality few-cycle output pulse with minimum energy spread across satellite pulses or pedestals. It is clear that, if one looks for such a post-compressed output, the second stage is the optimum regime. Simple diagnostics such as looking at the spectral broadening alone, which continues to increase in the third region, cannot be used to identify the optimum propagation conditions. Even though short temporal spikes may develop in this region, the overall temporal structure is complex, which strongly compromises the quality of the compression. The optimal propagation distance,  $z_{opt}$ , is therefore defined as the distance where we obtain the shortest stable less-structured post-compressed pulse within the second propagation stage. To identify  $z_{opt}$  we will look at the structure of the d-scan traces to unveil the temporal pulse structure from a global perspective, i.e., taking into account the actual capabilities of the compressor to properly compensate the output pulse phase.

The exact limits of the three identified propagation stages are somewhat flexible, but these stages, and also the optimal propagation distance, can always be identified in propagations with different gases and over a wide range of parameters. The propagation distance where each stage, as well as  $z_{opt}$ , appears can be controlled with both the input pulse parameters (energy, temporal duration, chirp, coupling conditions, among others) and gas parameters (gas type and pressure). One may use these parameters to locate the optimal propagation distance at the end of the HCF to have the desired outcome from the post-compression setup. For the parameters used in Fig. 1 we have denoted  $z_{opt}$  by vertical dashed green lines, indicating that the best setup under these conditions would be to have a HCF of length equal to this particular distance. For these particular cases, where the HCF is pumped by Fourier-limited 24 fs pulses,  $z_{opt}$  is around 50 cm. We also performed simulations for positively chirped input pulses, having observed the same dynamics and behavior, with the main difference being a shift in the position of  $z_{opt}$  towards longer distances. For the sake of simplicity, and without loss of generality, we restricted the present analysis to the case of Fourier-limited input pulses. It is worth mentioning that Fig. 1b) clearly shows that *the optimum output pulse is not the one with the broadest spectrum but the shortest among the*

less temporally-structured pulses obtained in the stable propagation stage, which we have been able to univocally identify through the resulting d-scan traces, as described in detail below.

### Identification of the optimum propagation distance ( $z_{opt}$ ) and the compressed pulse features. Comparison with experiments.

To locate  $z_{opt}$  we simulate the nonlinear propagation of the pulse followed by a d-scan compression/measurement stage of the on-axis far field at each propagation distance of the HCF. The d-scan compressor is composed of chirped mirrors followed by a pair of BK7 glass wedges, as in the d-scan setup commonly used for few-cycle pulse compression [43], but taking only into account their group delay dispersion effect and neglecting higher order terms. We assume ultra-broadband chirped mirrors, which introduce  $-100 \text{ fs}^2$  of pure GDD, with the BK7 wedges introducing  $44.65 \text{ fs}^2/\text{mm}$ . This simplification helps us identify the origin of the higher order dispersion terms that may appear in the pulse phase, which must come from the propagation in the HCF because the compression/measurement stage does not introduce them. We should note here that real CMs also introduce a given amount of negative TOD to compensate for the positive TOD of the gas, window and wedge materials, which means that the TOD that we have neglected in our compression/measurement stage (CMs and wedges) is indeed a good approximation of an actual experiment. Therefore, if we use the calibrated GDD and TOD dispersion of the CMs together with the complete dispersion of the BK7 wedges, the TOD observed in the d-scan trace should be basically the same as the one observed in our d-scan trace. Bearing in mind that the d-scan technique generates traces that are intuitively related to the dispersion orders imparted on the pulse, which are responsible for its temporal structure, we will be able to identify the global phase structure of the output pulse from the d-scan trace, based on the explanation given in the Introduction section.

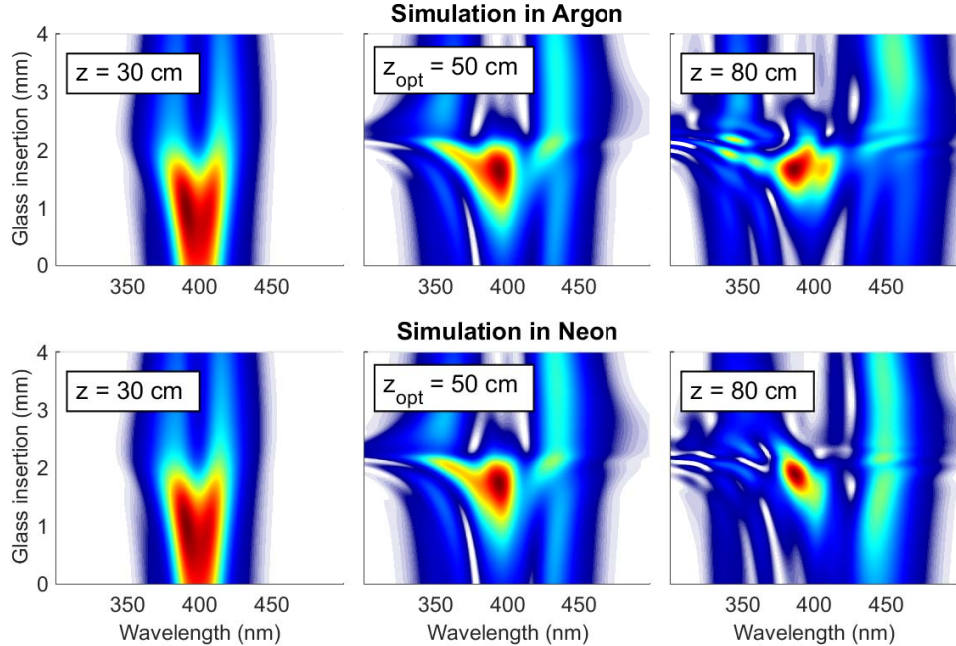


**Figure 2.** Simulated d-scan traces for argon at 0.5 bar (top row) and neon at 1.5 bar (bottom row) at the first stage ( $z=30 \text{ cm}$ , left plot), at the optimum propagation distance within the second stage ( $z_{opt}=50 \text{ cm}$ , middle plot), and at the complex third stage ( $z=80 \text{ cm}$ , right plot).

Figure 2 shows the d-scan traces at the three propagation positions denoted by vertical lines in Fig. 1 for the two considered gases. The top and bottom rows correspond to the argon and neon cases, respectively. Each column is located in a different propagation stage: the traces given in left column correspond to the start-up stage, where there is only a small spectral broadening. The central plots correspond to the  $z_{opt}$  region (in the second stage), where we have identified the optimum stable output pulse. For the parameters used in those

simulations we obtained a 3.7 fs temporal FWHM pulse duration for Ar and 3.3 fs FWHM for Ne for the wedge insertions that minimize the pulse duration (2.18 mm for Ar and 2.20 mm for Ne). It can be clearly seen that the optimum d-scan traces are almost identical for both gases, which is very helpful to identify  $z_{opt}$ . Finally, the plots on the right column are in the third propagation stage, showing a spectrally broader but extremely modulated trace that corresponds to strongly structured pulses. Although these last pulses present broader spectra, their phase structure is too complicated to be properly compensated for so as to generate few-cycle pulses. We present a movie (see Supplementary Material) showing the evolution of the d-scan trace and the wedge-insertion-dependent post-compressed pulse as a function of propagation distance in the HCF for the argon case shown in Fig. 2. The left plot in the movie shows the particular features of the d-scan trace along all the three stages. The right plot shows the final compressed pulse that can be obtained, displaying the continuous evolution of the structure of the pulse.

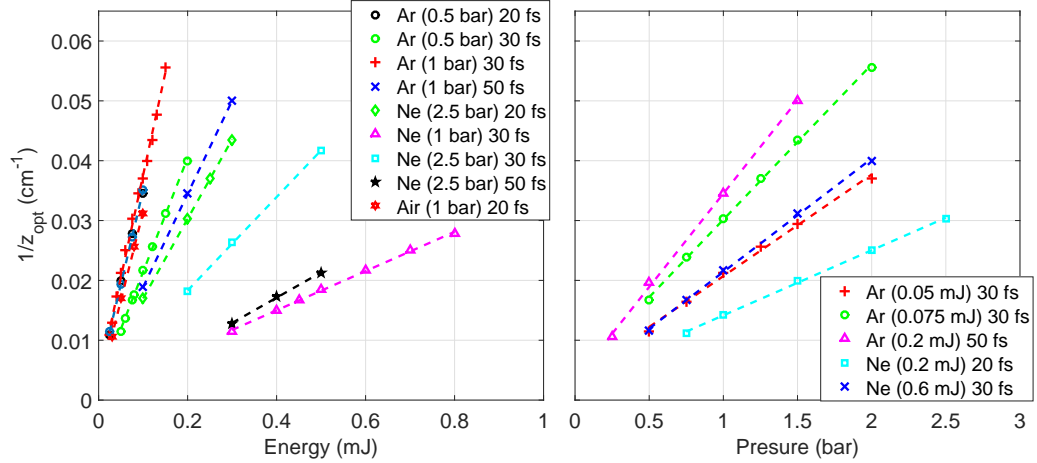


**Figure 3.** Dependence of  $1/z_{opt}$  with pulse energy (left) and gas pressure (right) for different representative pulse durations and gases. All input pulses are initially Fourier-limited.

Surprisingly, regardless of the input conditions, we have observed that the nonlinear dynamics always evolve towards the same optimum d-scan trace (Fig. 2, center column) at a certain propagation distance ( $z_{opt}$ ). This universal behavior, together with the particular d-scan trace at  $z_{opt}$  as a univocal fingerprint, is a very useful tool both for optimizing existing systems and to further promote the spreading of few-cycle pulse systems to many more applications that can benefit from a stable and reproducible source. Moreover, to unveil how  $z_{opt}$  varies with pulse and gas parameters, we performed simulations under different conditions, identifying the  $z_{opt}$  for each case. The obtained results are summarized in Fig. 3 and, although we are dealing with complex nonlinear processes, we observe a consistent and clearly scalable behavior. The results indicate that  $z_{opt}$  is inversely proportional to both pulse energy and gas pressure in all the situations that we have explored. This demonstrates the tunability of  $z_{opt}$  with respect to key parameters such as pressure, type of gas and input energy or pulse duration, setting this procedure as a universal route to obtain few-cycle pulses in the important visible-NIR spectral region.

In Fig. 4 we show examples of d-scan traces obtained experimentally to compare with those presented in Fig. 2. In this case we present traces for Ar at 0.15, 0.265 and 0.9 bar, shown in the left, middle and right plots, respectively, for a HCF of 100 cm length and 250  $\mu\text{m}$  diameter. Changing the gas pressure or the pulse energy yields similar results to using fibers of different lengths and is of course much easier to do in the laboratory. Another parameter that can be used to tune the output pulse is the chirp of the incident pulse, which can be varied in the compression stage of the laser system. An incident pulse with higher positive GDD will have a longer optimum distance  $z_{opt}$  while retaining similar propagation dynamics compared to the Fourier-limited and smaller GDD cases, as we have also verified in our simulations.

The comparison between theoretical and experimental results confirms the existence of the general behavior explained before, with the presence of an optimum propagation distance. This  $z_{opt}$  has a univocal d-scan trace with distinctive features, presenting always a slightly negative slope which corresponds to a negative TOD. This

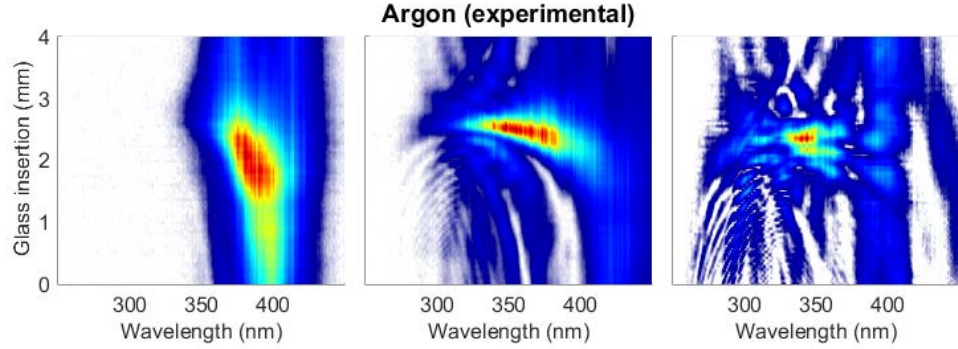


**Figure 4.** Experimental d-scan traces for a 25 fs, 1 mJ laser pulse in argon at the three different stages, observed for increasing values of the gas pressure: 0.15 bar (left), 0.265 bar (center) and 0.9 bar (right). The central d-scan represents an optimum configuration with similar characteristics to the theoretical case.

is the remaining residual TOD accumulated during the nonlinear propagation of the pulse inside the HCF. In the left plot of the movie (see Supplementary Material), where we present the evolution of the d-scan trace during propagation in the HCF, one can easily identify the region where the trace acquires a negative slope, indicating that we have reached  $z_{opt}$ . The region where the d-scan presents this particular feature extends over several centimeters, being relatively easy to find experimentally with the help of the d-scan trace, which shows exactly the same trend evidenced by the simulations. To our knowledge, this remaining TOD is present in all experimental HCF post-compressed pulses (in many cases it can be directly identified in the measured d-scan trace) obtained in different laboratories around the world when optimizing for the output pulse (United Kingdom [42], Portugal [41, 42], France [45], Sweden [46, 47], Germany [48], Canada [49], China [50], Austria [51] and United States of America [6, 39], as some examples). These experiments were done using HCFs with different characteristics (length and/or core diameter), filled with different gases (Ar, Ne or He) and with lasers in the NIR and mid-IR regions. All these observations support that the route to obtain an optimum post-compressed pulse described here is universal.

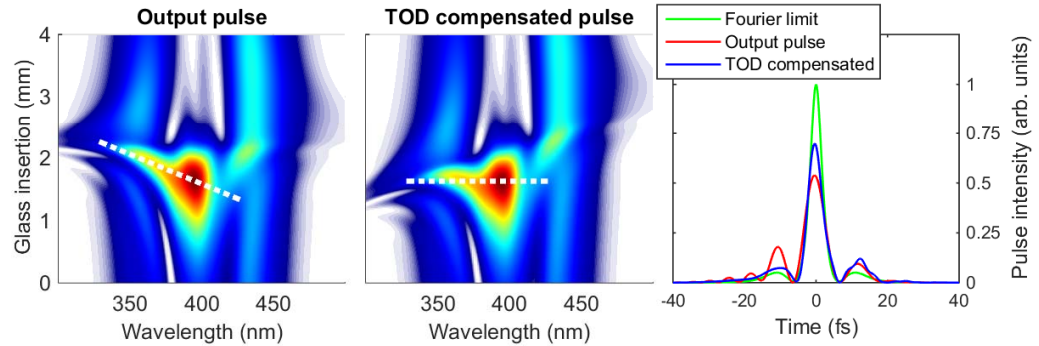


**Figure 5.** D-scan traces of (left) the optimum pulse for the simulation parameters of the top middle graph in Figure 2 (Ar-filled HCF with 0.5 bar pumped with Fourier-limited  $\sim 24$  fs pulses) and (middle) the same pulse with additional TOD compensation ( $+50$  fs<sup>3</sup>). The dashed white lines are a visual guide to see the change of slope in the trace associated to TOD compensation. (right) Output pulse in the time domain, before (red line) and after (blue line) TOD compensation. The Fourier-limited pulse (green line) is also shown for reference.

The residual TOD which appears in the optimal output pulses can be further compensated, not only to reduce the output pulse duration but also to increase the amount of energy in the output pulse. This can be done, for example, by using an adequate transparent medium such as water [41, 42, 46], z-cut KDP [44] or z-cut ADP [6], which directly enables achieving high-quality pulses in the single-cycle regime. In spite of its relatively small magnitude (e.g.,  $-40$  fs<sup>3</sup> reported in Ref. [41]), the effect of this TOD on a few- and single-cycle pulse can



be dramatic: its compensation enabled going from a 3.8 fs pulse to a near-transform-limited 3.2 fs 1.3-cycle pulse, which was accompanied by a significant improvement in pulse contrast and peak intensity [41]. In the center plot of figure 5 we show the d-scan trace obtained after compensating the residual TOD by adding +50 fs<sup>3</sup> in the measurement/compression stage, compared with the non-compensated case (left plot). We see that TOD compensation effectively tilts the d-scan trace so that its average negative slope practically disappears. To illustrate the improvement in energy throughput after TOD compensation we show on the right plot of Fig. 5 the direct output pulse and the TOD-compensated pulse, together with their Fourier Limit. The used glass insertion in this case is that which results in maximum intensity in the d-scan trace. Clearly, the pulse corresponding to the TOD-corrected trace has better characteristics: it presents an increase in peak intensity of the order of 30%, a reduction of the temporal FWHM pulse duration from 6.05 fs to 4.49 fs, getting much closer to the Fourier Limit case (3.52 fs), and smaller secondary temporal structures than the non-corrected case, as also confirmed by experiments.

## Conclusion

In this work we have presented and analyzed a route to obtain optimum hollow-core fiber post-compressed pulses using the d-scan setup as the compression and diagnostic device. We have demonstrated that by changing the gas pressure and/or input pulse energy, one is able to identify the optimal post-compression parameters to obtain the shortest less-structured and stable output pulses. This optimal setup can be univocally identified by the d-scan trace of the output pulses, which shows a marked TOD feature, whereas overdriving the HCF above this optimum regime invariably results in an increasingly complex nonlinear spectral phase, partly due to plasma onset, which renders compression very hard to optimize. For the optimum propagation region, the remaining TOD can be further compensated, for example by simple linear propagation in an adequate transparent medium, which improves the temporal shape and the peak power of the output pulse. The identified propagation regime and approach enable the generation of stable and high-quality few- to single-cycle pulses, which has direct implications in the performance of current and new HCF pulse post-compression systems and will help improve and extend the applications of these extreme light sources in many fields of science and technology.

## Methods

**Simulations.** To study the nonlinear propagation of a laser pulse in a HCF we have implemented the standard nonlinear envelope propagation equation [52]. The model includes the spatial and temporal pulse dynamics. We use a local frame moving with the pulse  $T = t - z/v_g$ , being  $v_g$  the group velocity of the pulse, and assume cylindrical symmetry. The propagation equation for the temporal envelope of the pulse,  $A(r, z, T)$ , is

$$\frac{\partial A(r, z, T)}{\partial z} = (\hat{L} + \hat{N})A(r, z, T). \quad (1)$$

The first part of the propagation equation,  $\hat{L}$ , represents the linear propagation effects: diffraction, dispersion and linear losses. The other part,  $\hat{N}$ , represents the nonlinear propagation effects, which include self-phase modulation, Raman scattering, ionization, losses due to the ionization process and plasma absorption, and self-steepening.

To solve Eq. 1 we use a split-step method dividing each propagation step into two sub-steps [53]. The first one consists on applying only the linear effects by decomposing the input pulse into the  $EH_{1m}$  modes of the hollow-core fiber [54, 55]

$$\tilde{A}(r, z, \omega) = \sum_{m=1}^{\infty} c_m(\omega, z) EH_{1m}(r), \quad (2)$$

where  $\tilde{A}(r, z, \omega)$  represents the Fourier Transform of  $A(r, z, T)$ . The coefficients of the decomposition can be calculated by doing the inverse Hankel Transform of the spatial beam distribution in the core of the HCF

$$c_m(\omega, z) = \frac{1}{a^2 J_1^2(\alpha_m)} \int_0^a \tilde{A}(r, z, \omega) J_0\left(\alpha_m \frac{r}{a}\right) r dr, \quad (3)$$



being  $a$  the core radius of the HCF and  $\alpha_m$  the  $m^{th}$ -zero of  $J_0(x)$ , where  $J_\nu$  is the Bessel function of the first kind of order  $\nu$ . We solve Eq. 3 by using the discrete Hankel Transform scheme proposed in [56]. The complete linear propagation in the HCF is simulated by using the complex propagation coefficient of each mode,  $\beta_m(\omega)$ , [54], as shown in Eq. 4. The real and imaginary parts of  $\beta_m(\omega)$  take into account all the dispersion and losses of the  $m^{th}$ -mode of the HCF, respectively

$$\tilde{A}(r, z + \Delta z, \omega) = \sum_{m=1}^{\infty} c_m(\omega, z) E H_{1m}(r) \exp(i\beta_m(\omega)\Delta z). \quad (4)$$

The second sub-step of the method consists in applying the nonlinear effects. Separating  $\hat{N}[A(r, z, T)] = N_{SPM}(A) + N_{ioniz}(A) + N_{abs}(A)$ , a mathematical expression for each term can be obtained [52], as given below. For the self-phase modulation, Raman scattering and self-steepening, we have

$$N_{SPM}(A) = ik_0 n_2 \left(1 + \frac{i}{\omega_0} \frac{\partial}{\partial T}\right) \left(A(r, z, T) \int_{-\infty}^T K(T-t) |A(r, z, T)|^2 dt\right). \quad (5)$$

In Eq. 5  $k_0 = n_0 2\pi/\lambda_0$ , with  $\lambda_0$  the central wavelength of the pulse.  $n_2$  the nonlinear refractive index,  $\omega_0 = 2\pi c/\lambda_0$  and  $K(T-t)$  representing the SPM together with the Raman scattering, which has the following form  $(1-x)\delta(T-t) + x/\tau_K \exp(-(T-t)/\tau_K)$ , where  $x$  is the ratio between the SPM and the Raman effect, and  $\tau_K$  fs is the characteristic time for the Raman response. For the ionization, we have

$$N_{ioniz}(A) = -\frac{\sigma}{2} (1 + i\omega_0 \tau_C) \left(1 + \frac{i}{\omega_0} \frac{\partial}{\partial T}\right)^{-1} [\rho(r, T) A(r, z, T)], \quad (6)$$

where  $\sigma$  is the cross section for the inverse Bremsstrahlung that depends on the collision time ( $\tau_C$ ), the critical density of the medium and the central frequency of the laser pulse [52].  $\rho$  represents the ionized electron density, whose evolution is governed by  $\partial\rho/\partial t = W(|A|^2)(\rho_{at} - \rho)$ , where  $W(|A|^2)$  is the ionization rate calculated using the PPT model [57] and  $\rho_{at}$  is the atomic density of the medium. Finally, the absorption term is

$$N_{abs}(A) = -\frac{W(|A|^2)U_i}{2|A|^2}(\rho_{at} - \rho), \quad (7)$$

where  $U_i$  represents the ionization potential of the gas.

Once we have calculated the spatio-temporal field distribution along the propagation inside the HCF, we calculate the different beam, and also gas, properties (spatial width, temporal duration, spectral bandwidth and maximum electron density) which enable a more complete view of the laser evolution inside the HCF. We plotted such properties in Fig. 1 for some particular cases to identify the main propagation stages. In order to be as close as possible to actual experimental conditions, we have averaged the distributions in the temporal or spatial coordinate, depending on the property. The spatial width was calculated from the beam fluence, obtained by integrating the spatio-temporal beam intensity over the temporal coordinate. The temporal duration and the spectral bandwidth are calculated from the incoherent spatial integration of the laser intensity distribution around the center of the HCF. By doing this we take into account not only the on-axis properties but also the beam properties over a wider region, being closer to the experimental situation in which the central part of the laser beam is usually selected with an aperture and then focused to be measured or to be used in an experiment. Regarding the maximum electron density, we have calculated its mean value around the center of the HCF. The criterion used to calculate the temporal duration, the spectral bandwidth and the maximum electron density consisted in integrating over a radius of 25  $\mu\text{m}$  around the HCF center.

To calculate the theoretical d-traces, such as those in Fig. 2, we have also mimicked the experimental procedure, by first selecting the part of the beam around the center of the HCF, using the same criterion indicated above, and then calculating its far field distribution via the Hankel transform. We have used the obtained on-axis far field to simulate the dispersion scan and generate the corresponding traces.

**Experiments.** The experiments were performed by employing 23 fs input laser pulses centered at 780 nm. These pulses were generated with a 1 kHz Ti:Sapphire CPA laser system (Femtolasers FemtoPower CompactPRO

---

HE CEP) which is part of the CLPU facility. The maximum pulse energy available was 2.5 mJ and we adjusted it to 1 mJ in our experiments. The laser pulses were focused by a spherical mirror (1 m focal length) into a hollow-core fiber (HCF) with an inner diameter of 250 micrometers and 1 meter length. The HCF was filled with argon gas at different pressures. Output pulses were compressed and measured using the d-scan technique from Sphere Ultrafast Photonics. In the d-scan setup we used a double-angle chirped mirror set (Ultrafast Innovations GmbH) and two motorized BK7 wedges to induce the dispersion scan.

## Acknowledgments

We acknowledge funding from the following institutions: Junta de Castilla y León (Project SA116U13, SA046U16); MINECO (FIS2013-44174-P, FIS2015-71933-REDT, FIS2016-75652-P); Fundação para a Ciência e a Tecnologia, Portugal, (Grants UID/NAN/50024/2013, NORTE-07-0124-FEDER-000070); Consejo Nacional de Ciencia y Tecnología, México (CONACYT México for Postdoctoral Research Fellowships). CLPU is acknowledged for granting access to its facilities.

## References

1. M. Hentschel, R. Kienberger, C. Spielmann, G. A. Reider, N. Milosevic, T. Brabec, P. Corkum, U. Heinzmann, M. Drescher, and F. Krausz, "Attosecond metrology," *Nature* **414**, 509-513 (2001).
2. M. F. Kling, and M.J.J. Vrakking, "Attosecond electron dynamics," *Annu. Rev. Phys. Chem.* **59**, 463-492 (2008).
3. F. Krausz, and M. Ivanov, "Attosecond physics," *Rev. Mod. Phys.* **81**, 163-264 (2009).
4. L. Gallmann, C. Cirelli, and U. Keller, "Attosecond science: recent highlights and future trends," *Annu. Rev. Phys. Chem.* **63**, 447-469 (2012).
5. F. Krausz, and M. I. Stockman, "Attosecond metrology: from electron capture to future signal processing," *Nat. Photonics* **8**, 205-213 (2014).
6. H. Timmers, Y. Kobayashi, K.F. Chang, M. Reduzzi, D.M. Neumark, and S.R. Leone, "Generating high-contrast, near single-cycle waveforms with third-order dispersion compensation," *Opt. Lett.* **42**, 811-814 (2017).
7. G. Sansone, E. Benedetti, F. Calegari, C. Vozzi, L. Avaldi, R. Flammini, L. Poletto, P. Villoresi, C. Altucci, R. Velotta, S. Stagira, S. De Silvestri, and M. Nisoli, "Isolated single-cycle attosecond pulses," *Science* **314**, 443-446 (2006).
8. D. Polli, M.R. Antognazza, D. Brida, G. Lanzani, G. Cerullo, and S. De Silvestri, "Broadband pump-probe spectroscopy with sub-10-fs resolution for probing ultrafast internal conversion and coherent phonons in carotenoids," *Chem. Phys.* **350**, 45-55 (2008).
9. M. Liebel, C. Schnedermann, T. Wende, and P. Kukura, "Principles and applications of broadband impulsive vibrational spectroscopy," *J. Chem. Phys. A* **119**, 9506-9517 (2015).
10. J. Du, J. Harra, M. Virkki, J.M. Mäkelä, Y. Leng, M. Kauranen, and T. Kobayashi, "Surface-enhanced impulsive coherent vibrational spectroscopy," *Sci. Rep.* **6**, 36471 (2016).
11. P. Kukura, D.W. McCamant, and R.A. Mathies, "Femtosecond stimulated Raman spectroscopy," *Annu. Rev. Phys. Chem.* **58**, 461-488 (2007).
12. T. Fujisawa, H. Kuramochi, H. Hosoi, S. Takeuchi, and T. Tahara, "Role of coherent low-frequency motion in excited-state proton transfer of green fluorescent protein studied by time-resolved impulsive stimulated Raman spectroscopy," *J. Am. Chem. Soc.*, **138**, 3942-3945 (2016).

13. D.R. Dietze, and R.A. Mathies, "Femtosecond stimulated Raman spectroscopy," *ChemPhysChem* **17**, 1224-1251 (2016).
14. H. Kuramochi, Sa. Takeuchi, and T. Tahara, "Femtosecond time-resolved impulsive stimulated Raman spectroscopy using sub-7-fs pulses: Apparatus and applications," *Rev. Sci. Instrum.* **87**, 043107 (2016).
15. Y.-T. Wang, M.-H. Chen, C.-T. Lin, J.-J. Fang, C.-J. Chang, C.-W. Luo, A. Yabushita, K.-H. Wu, and T. Kobayashi, "Use of ultrafast time-resolved spectroscopy to demonstrate the effect of annealing on the performance of P3HT:PCBM solar cells," *ACS Appl. Mater. Interfaces* **7**, 4457–4462 (2015).
16. C.-W. Luo, Y.-T. Wang, A. Yabushita, and T. Kobayashi, "Ultrabroadband time-resolved spectroscopy in novel types of condensed matter," *Optica* **3**, 82-92 (2016).
17. C. Schnedermann, J. M. Lim, T. Wende, A.S. Duarte, L. Ni, Q. Gu, A. Sadhanala, A. Rao, and P. Kukura, "Sub-10 fs time-resolved vibronic optical microscopy," *J. Phys. Chem. Lett.* **7**, 4854-4859 (2016).
18. Y. Nishiyama, K. Imura, and H. Okamoto, "Observation of plasmon wave packet motions via femtosecond time-resolved near-field imaging techniques," *Nano Lett.* **15**, 7657-7665 (2015).
19. J. Darmo, T. M'uller, W. Parz, J. Kr'oll, G. Strasser, and K. Unterrainer, "Few-cycle terahertz generation and spectroscopy of nanostructures," *Phil. Trans. R. Soc. Lond. A* **362**, 251-262 (2004).
20. J. Seres, A. Muller, E. Seres, K. O'Keeffe, M. Lenner, R. Herzog, D. Kaplan, C. Spielmann, and F. Krausz, "Sub-10-fs, terawatt-scale Ti : sapphire laser system," *Opt. Lett.* **28**, 1832-1834 (2003).
21. G. Cerullo, M. Nisoli, S. Stagira, and S. De Silvestri, "Sub-8-fs pulses from an ultrabroadband optical parametric amplifier in the visible," *Opt. Lett.* **23**, 1283-1285 (1998).
22. M. Miranda, C.L. Arnold, T. Fordell, F. Silva, B. Alonso, R. Weigand, A. L'Huillier and H. Crespo, "Characterization of broadband few-cycle laser pulses with the d-scan technique," *Opt. Express* **20**, 18732 (2012).
23. V. Cardin, N. Thiré, S. Beaulieu, V. Wanie, F. Légaré and B.E. Schmidt, "0.42 TW 2-cycle pulses at 1.8  $\mu\text{m}$  via hollow-core fiber compression," *Appl. Phys. Lett.* **107**, 181101 (2015).
24. W. J. Tomlinson, R. H. Stolen, and C. V. Shank, "Compression of optical pulses chirped by self-phase modulation in fibers," *J. Opt. Soc. Am. B* **1**, 139-149 (1984).
25. R. Fork, C. Cruz, P. Becker, and C. Shank, "Compression of optical pulses to 6 femtoseconds by using cubic phase compensation," *Opt. Lett.* **12**, 483-485 (1987).
26. M. Nisoli, S. DeSilvestri and O. Svelto, "Generation of high energy 10 fs pulses by a new pulse compression technique," *Appl. Phys. Lett.* **68**, 2793 (1996).
27. S. Sartania, Z. Cheng, M. Lenzner, G. Tempea, Ch. Spielmann, F. Krausz, and K. Ferencz, "Generation of 0.1-TW 5-fs optical pulses at a 1-kHz repetition rate," *Opt. Lett.* **22**, 1562-1564 (1997).
28. C. P. Hauri, W. Kornelis, F. W. Helbing, A. Heinrich, A. Couairon, A. Mysyrowicz, J. Biegert, and U. Keller, "Generation of intense, carrier-envelope phase-locked few-cycle laser pulses through filamentation," *Appl. Phys. B-Lasers and Optics* **79**, 673-677 (2004).
29. A. Blättermann, C. Ott, A. Kaldun, T. Ding, V. Stooi, M. Laux, M. Rebholz, and T. Pfeifer, "In situ characterization of few-cycle laser pulses in transient absorption spectroscopy," *Opt. Lett.* **40**, 3464-3467 (2015).
30. A. Schiffrin, T. Paasch-Colberg, N. Karpowicz, V. Apalkov, D. Gerster, S. M'hlbrandt, M. Korbman, J. Reichert, M. Schultze, S. Holzner, J.V. Barth, R. Kienberger, R. Ernstorfer, V.S. Yakovlev, M.I. Stockman, and F. Krausz, "Optical-field-induced current in dielectrics," *Nature* **493**, 70-74 (2013).

31. M. Schultze, E.M. Bothschafter, A. Sommer, S. Holzner, W. Schweinberger, M. Fiess, M. Hofstetter, R. Kienberger, V. Apalkov, V.S. Yakovlev, M.I. Stockman, and F. Krausz, "Controlling dielectrics with the electric field of light," *Nature* **493**, 75-78 (2013).
32. I. A. Bocharova, A.S. Alnaser, U. Thumm, T. Niederhausen, D. Ray, C. L. Cocke, and I. V. Litvinyuk, "Time-resolved Coulomb-explosion imaging of nuclear wave-packet dynamics induced in diatomic molecules by intense few-cycle laser pulses," *Phys. Rev. A* **83**, 013417 (2011).
33. J. Liu, K. Okamura, Y. Kida, T. Teramoto, and T. Kobayashi, "Clean sub-8-fs pulses at 400 nm generated by a hollow fiber compressor for ultraviolet ultrafast pump-probe spectroscopy," *Opt. Express* **18**, 20645-20650 (2010).
34. J. Liu, A. Yabushita, S. Taniguchi, H. Chosrowjan, Y. Imamoto, K. Sueda, N. Miyanaga, and T. Kobayashi, "Ultrafast time-resolved pump-probe spectroscopy of PYP by a sub-8 fs pulse laser at 400 nm," *J. Phys. Chem. B* **117**, 4818-4826 (2013).
35. T. Kobayashi, and Y. Kidaw, "Ultrafast spectroscopy with sub-10 fs deep-ultraviolet pulses," *Phys. Chem. Chem. Phys.* **14**, 6200-6210 (2012).
36. M. Gueye, J. Nillon, O. Cregut, and J. Léonard, "Broadband UV-Vis vibrational coherence spectrometer based on a hollow fiber compressor," *Rev. Sci. Instrum.* **87**, 093109 (2016).
37. M. Paolino, M. Gueye, E. Pieri, M. Manathunga, S. Fusi, A. Cappelli, L. Latterini, D. Pannacci, M. Filatov, J. Léonard, and M. Olivucci, "Design, synthesis, and dynamics of a green fluorescent protein fluorophore mimic with an ultrafast switching function," *J. Am. Chem. Soc.*, **138**, 9807-9825 (2016).
38. C.S. Gonçalves, A.S. Silva, D. Navas, M. Miranda, F. Silva, H. Crespo, and D.S. Schmool, "A dual-colour architecture for pump-probe spectroscopy of ultrafast magnetization dynamics in the sub-10-femtosecond range", *Sci. Rep.* **6**, 22872 (2016).
39. H.-T. Chang, M. Zürich, P.M. Kraus, L.-J. Borja, D.M. Neumark and S.R. Leone, "Simultaneous generation of sub-5-femtosecond 400 nm and 800 nm pulses for attosecond extreme ultraviolet pump-probe spectroscopy", *Opt. Lett.* **41**, 5365-5368 (2016).
40. D. Guénot, D. Gustas, A. Vernier, B. Beaupaire, F. Böhle, M. Bocoum, M. Lozano, A. Jullien, R. Lopez-Martens, A. Lifschitz and J. Faure, "Relativistic electron beams driven by kHz single-cycle light pulses" arXiv:1611.09543 [physics.plasm-ph].
41. F. Silva, M. Miranda, B. Alonso, J. Rauschenberger, V. Pervak, and H. Crespo, "Simultaneous compression, characterization and phase stabilization of GW-level 1.4 cycle VIS-NIR femtosecond pulses using a single dispersion-scan setup," *Opt. Express* **22**, 10181-10190 (2014).
42. D. Fabris, W. Holgado, F. Silva, T. Witting, J.W.G. Tisch and H. Crespo, "Single-shot implementation of dispersion-scan for the characterization of ultrashort laser pulses," *Opt. Express* **23**, 32803-32808 (2015).
43. M. Miranda, T. Fordell, C. Arnold, A. L'Huillier, and H. Crespo, "Simultaneous compression and characterization of ultrashort laser pulses using chirped mirrors and glass wedges," *Opt. Express* **20**, 688-697 (2012).
44. M. Miranda, J. Penedones, C. Guo, A. Harth, M. Louisy, L. Neoricic, A. L'Huillier, and C. L. Arnold, "Fast iterative retrieval algorithm for ultrashort pulse characterization using dispersion scan," *J. Opt. Soc. Am. B* **34**, 1190-1197 (2017).
45. F. Bohle, M. Kretschmar, A. Jullien, M. Kovacs, M. Miranda, R. Romero, H. Crespo, U. Morgner, P. Simon, R. Lopez-Martens, and T. Nagy, "Compression of CEP-stable multi-mJ laser pulses down to 4 fs in long hollow fibers," *Las. Phys. Lett.* **11** 095401 (2014).

46. M. Louisy, C.L. Arnold, M. Miranda, E.W. Larsen, S.N. Bengtsson, D. Kroon, M. Kotur, D. Guénot, L. Rading, P. Rudawski, F. Brizuela, F. Campi, B. Kim, A. Jarnac, A. Houard, J. Mauritsson, P. Johnsson, A. L'Huillier and C.M. Heyl, "Gating attosecond pulses in a noncollinear geometry," *Optica* **2** 563-566 (2015) (Supplementary Material).
47. C. M. Heyl, H. Coudert-Alteirac, M. Miranda, M. Louisy, K. Kovacs, V. Tosa, E. Balogh, K. Varjú, A. L'Huillier, A. Couaïron, and C. L. Arnold, "Scale-invariant nonlinear optics in gases," *Optica* **3**, 75-81 (2016) (Supplementary Material).
48. A. Tajalli, B. Chanteau, M. Kretschmar, H.G. Kurz, D. Zuber, M. Kovacev, U. Morgner and T. Nagy, "Few-cycle optical pulse characterization via cross-polarized wave generation dispersion scan technique," *Opt. Lett.* **41**, 5246-5249 (2016).
49. B. E. Schmidt, et al. "Compression of 1.8  $\mu\text{m}$  laser pulses to sub two optical cycles with bulk material," *Appl. Phys. Lett.* **96**, 121109 (2010).
50. Z. Huang, D. Wang, Y. Dai, Y. Li, X. Guo, W. Li, Y. Chen, J. Lu, Z. Liu, R. Zhao and Y. Leng, "Design of intense 1.5-cycle pulses generation at 3.6  $\mu\text{m}$  through a pressure gradient hollow-core fiber," *Opt. Express* **24**, 9280-9287 (2016).
51. G. Fan, T. Balciunas, T. Kanai, T. Flöry, G. Anriukaitis, B.E. Schmidt, F. Légaré and A. Baltuska, "Hollow-core-waveguide compression of multi-millijoule CEP-stable 3.2  $\mu\text{m}$  pulses," *Optica* **3**, 1308-1311 (2016).
52. A. Couaïron, and A. Mysyrowicz, "Femtosecond filamentation in transparent media," *Phys. Rep.* **441**, 47-189 (2007).
53. G.P. Agrawal, "Nonlinear Fiber Optics," 3rd Ed. (Academic Press, San Diego, 2001).
54. E. Marcatili and R. Schmeltzer, "Hollow metallic and dielectric waveguides for long distance optical transmission and lasers," *Bell Syst. Tech. J.* **43**, 1783-1809 (1964).
55. E. Granados, L. Chen, C. Lai, K. Hong, and F. Kartner, "Wavelength scaling of optimal hollow-core fiber compressors in the single-cycle limit," *Opt. Express* **20**, 9099-9108 (2012).
56. M. Guizar-Sicairos and J.C. Gutierrez-Vega, "Computation of quasi-discrete Hankel transforms of integer order for propagating optical wave fields," *J. Opt. Soc. Am. A* **21**, 53 (2004).
57. A.M. Peremolov, V.S. Popov and M.V. Terentev, "Ionization of atoms in an alternating electric field," *Sov. Phys. JETP* **23**, 924 (1966).